View metadata, citation and similar papers at core.ac.uk
brought to you by CORE
provided by UPCommons. Portal del coneixement obert de la UPC

Behaviour of the anomalous regions of the Continuous Shouldered Well isotropic soft-core potential

Pol Vilaseca Mainar
directed by
Giancarlo Franzese
Departament de Física Fonamental, Facultat de Física, Universitat de Barcelona, Diagonal 647, 08028, Barcelona, Spain

14 September 2009

Abstract

Using molecular dynamics we simulate a system of particles interacting through a continuous isotropic pairwise core-softened potential, proposed by Franzese [1], consisting on a repulsive shoulder and an attractive well. The model is known to display a phase diagram with three fuid phases with a gas-liquid critical point and liquid-liquid critical point and to present density, diffusion and structural anomalies, in the same hierarchy that characterizes water. In this work we increase systematically the slope of the repulsive shouder to study the effect on the anomalies. We find that the different anomalous regions are sensible to the changes and get narrow as the slope increases. While diffusion and density anomalous regions tend to colapse into one single point in the $T-\rho$ plane, structural anomalous region tends asimptotically to a fixed value.

1 Introduction

Several liquids exhibit anomalous behaviours which are not well understood. Water is the most common example of such systems. Although it is an abundant substance in earth and elementary for life, the mechanisms that govern its behaviour are still an open problem. Literature reports up to sixty-one anomalies.

Normal liquids contract when they are cooled. Water expands under $T = 4^oC$ at ambient pressure [2]. Experimets for Bi [3], Ga [3], Te [4], S [5], [6], $Ge_{15}Te_{85}$ [7] and simulations for silica[8]–[11], silicon [12] and BeF_2 [8] also reveal this behaviour. This systems present a temperature of maximum density (TMD) bellow which density decreases when temperature is lowered at constant pressure.

Dynamics of water is also anomalous. Commonly, the diffusivity of a system decreases as density or pressure is increased. In the case of water, instead by increasing the pressure increases the diffussion coefficient D for a wide range of the phase diagram. Expreriments show how its normal behaviour is not restored until high pressures are reached (e.g. for $P \approx 1.1$ kbar at $283K$) [2].

The structure of the system and the anomalies are deeply related. Errington and Debendetti [14] used two order parameters for studying the behaviour of the structure under compression, namelly, a translational order parameter t which quantifies the tendency of pairs of molecules to adopt preferential separations, and an orientational order parameter q that measures the tendency of a molecule to assume a tetrahedral arrangement with its four nearest neighbours ocupying a vertex. Steinhardt *et al* introduced another familly of orientational order parameters Q_l [14], which depend on the number of nearest neighbours for each molecule, used to study other network arrangements. Normal liquids tend to become more structurated when compressed so t and q (or Q_l) increase with pressure. Water and anomalous liquids, however, show a region for which the structural order parameters decrease with pressure. In this structural anomalous region the system becomes more disordered until the normal behaviour is restored. The sequence of anomalies in the phase diagram is different for different systems. For the $T-\rho$ phase diagram of water the structural anomalous region is encompassing the diffusion anomalous region which includes the density anomaly region. For silica, the difussion anomalous region contains the structural anomaly and the later the density anomalous region [10]. It has been shown that the model studied in this paper shares water's hierarchy of anoamalies [1],[15].

Many detailed models of water have been proposed in order to describe its behaviour and reproduce the previous anomalies [16]–[18]. However, detailed models tend to be complicated and cannot be easily generalized to other systems, bringing light to the physical mechanisms that lay behind the anomalies.

Isotropic models are a simple aproach to understand anomalous behaviours for fluids. This models consist in a system of identical particles interacting through a potential composed of a repulsive core with a region of softening that can either be a ramp or a shoulder [19]–[32].

In this work we investigate the presence of anomalies in the Continous Shoudered Well potential (CSW), introduced by Franzese [1], and their dependence on the softness of the repulsive shoulder.

This report is organized as follows. The model under study is presented in Sec 2. Details of the simulations are found in Sec 3. In sections 4-5 we present the phase diagram and the anomalies found, respectivelly. Finally, in Sec 6, we summarize and give the conclusions of the work.

2 The Model

We study the Continuous Shouldered-Well (CSW) model proposed in Ref. [1] and consisting of a set of identical particles interacting through the isotropic pairwise potential given by

$$U(r) = \frac{U_R}{1 + exp\left(\Delta(r - R_R)/a\right)} - U_A \times exp\left[-\frac{(r - R_A)^2}{2\delta_A^2}\right] + \left(\frac{a}{r}\right)^{24} \quad (1)$$

where a is the diameter of the particles, R_A and R_R are the distance of the attractive minimum and the repulsive average radius, U_A and U_R are the energies of both the attractive well and repulsive shoulder, δ_A^2 is the variance of the Gaussian centered at R_A, and Δ is the parameter which controles the slope between the shoulder and the well at R_R. Varying the parameters the potential can be tuned from a repulsive shoulder to a deep double well.

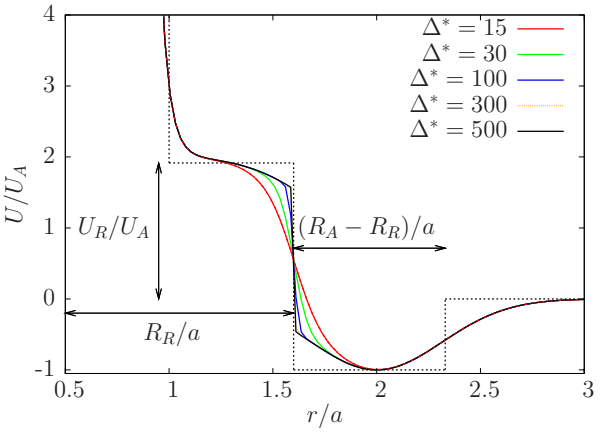

Figure 1: Continuous colour lines represent the different pairwise interaction potentials studied in this work (CSW). Solid black line represents the discountinuous shouldered well potential (DSW)[33]−[36] associated to the cotinuous one. A detailed comparation of both potentials is performed by Franzese [ref Franzese] and Barros de Oliveira [ref Alan]. By increasing the values of Δ, parameter that controls the slope at R_R, it is possible to move from a smooth version of the continuous potential to the limiting case where we almost reach a discontinuity at distance $R_R/a = 1.6$ as in the discontinuous potential.

This model is known to present anomalies in density, diffusion and structure and also liquid-gas and liquid-liquid phase transitions both ending in critical points [1],[15]. The CSW is the first potential incorporing a strong shoulder that displays waterlike anomalies, making it specially suitable for studying liquid metals (Cs, Mg, Sr, Ba) and colloids. The set of values chosen for the simulations are [1],$U_R/U_A = 2$, $R_R/a = 1.6$, $(\delta_A/a)^2 = 0.1$. We study different values of the parameter $\Delta^* \equiv \Delta/a = 15, 30, 100, 300, 500$ (Fig. 2) in order to explore how the anomalous regions change with the slope Δ^*, going from the case $\Delta^* = 15$ studied in Ref. [1],[15] to higher slopes, aproaching the discontinuous case.

No matter which value of Δ^* we select, the potential $U(r) \to 0$ for distances $r/a > 3$ hence, in order to reduce the computational effort, we establish a cuttoff distance at $r_c = 3.0a$.for $U(r)$.

3 Details of simulations

We simulate the behaviour of the system governed by the CSW potential using standard molecular dynamics thechniques for continuous potentials [37]. We perform simulations in the NVT ensemble for $N = 1372$ particles interacting in a cubic box of volume V with periodic boundary conditions at temperature T. We use a simple Allen thermostat keeping T constant by reescaling the velocities of the particles at each time step by a factor $(T/\mathcal{T})^{\frac{1}{2}}$, where $\mathcal{T}$ is the instantaneous kinetic temperature and T the fixed temperature of the thermal bath [38]. We integrate the equations of motion using velocity Verlet integrator [38]. By fixing ρ and T, we calculate the pressure in terms of the second virial coefficient [38]. All calculations are done in dimensionless reduced units in terms of the particle diameter and the depth of the attractive well: $P^* \equiv Pa^3/U_A$, $T^* \equiv k_B T/U_A$, $\rho^* \equiv \rho a^3$, and $D^* \equiv D(m/a^2 U_A)^{1/2}$ for diffusion constant D.

We use a time step of $\delta t^* = 3.2 \times 10^{-3}$ defined in units of $(a^3 m/U_A)^{1/2}$ (of the order of $\approx 1.7 \times 10^{-12} s$ for water-like molecules and $\approx 2.1 \times 10^{-12} s$ for argon-like atoms). Simulations are performed for 10^6 time steps for each run plus 10^4 for equilibration purposes. Positions and velocities are stored every 1000 time steps and kept for calculating structure and dynamics. The values for pressure and energy are computed every 100 time steps. For each value of ρ^* and T^* we repeat each run twice, starting from different initial configurations and keeping the mean of the observables computed in both runs. Averages taken within the metaestable regions (see next section) are performed by quenching from higher temperatures and stopping the run once the configurational energy has a sudden change. The lifetime of the metaestable phase is characterized by the time between the end of the equilibration and the energy drop. This process is repeated for every chosen value of Δ^*.

4 The phase diagram

We generate a set of isotherms in the $p - \rho$ phase diagram for every value of Δ^*, finding similar behaviours for all cases under study (the case $\Delta^* = 30$ is displayed in Fig. 2) [1]. High temperature isotherms grow monothonically when increasing ρ^*, while low temperature isotherms present two loops, characteristic of first order phase transitions. The lines formed joining the minima and maxima of the loops are an estimation of the branches of the spinodal line. Each branch corresponds to the limit of stability of one of the

coexisting phases involved in the first order phase transition. The point where the two branches meet is by definition the critical point where the transition ends. The critical isotherms in the critical points accomplish $\left(\partial^2 p/\partial\rho^2\right)_{T_c} = 0$. Above this point isotherms increase monothonically.

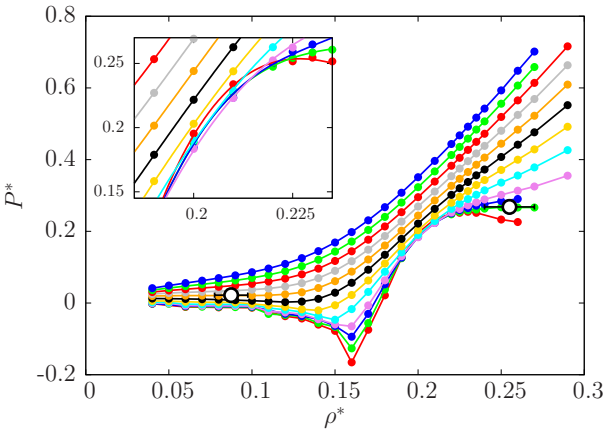

Figure 2: $P^* - \rho^*$ projection of the phase diagram for $\Delta^* = 30$. Low temperature isotherms have no longer a monothonic behaviour and show two van der Waals loops, corresponing to a liquid-gas (low densities) and a liquid-liquid (higher densities) first order phase transitions both ending in critical points (empty circles). Isotherms are, from bottom to top, at $T^* = 0.45$, 0.5, 0.55, 0.6, 0.7, 0.8, 0.9, 1.0, 1.1, 1.2, 1.3, 1.4, 1.5, 1.7 and 1.9. Inset: the crossing of the isotherms signals the presence of a density anomally. Errors, where not shown, are smaller than point sizes.

The two loops for every value of Δ^* appear in a low density regime and in a high density regime and correspond to a gas-liquid phase transition (G-L) and a liquid-liquid (L-L) phase transition respectivelly, this last between a low density liquid phase (LDL) and a high density liquid (HDL). The HDL is strongly metastable with respect to the crystal phase and spontaneous crystalization difficults the study of the region around the L-L critical point, where nucleation precess occurs very fast. However, data in this region can be obtained from the interpolation of higher temperature isotherms. Estimations of the critical points for each value of Δ^* and for the limiting case of the discontinuous potential are shown in Table 1. As Δ^* is increased and the slope of the potential is variated from being smooth to the almost discontinuous case, both G-L and L-L critical points move continuosly and tend to the values corresponding to the discontinuous potential (Fig. 1), which is in accordance to the hipothesis of the DSW being a limiting case of the familly of CSW potentials given by Eq (1). However, critical temperature and pressure for the L-L critical point corresponding to $\Delta^* = 500$ (the highest value for Δ^* studied in this work) are still distanced from the values of the DSW potential. For densities around the L-L critical point, low-temperature isotherms cross marking the presence of an anomally in density (see Sec 5.1). The region with the crossing isotherms contracts as the value of Δ^* increases until it almost disappears for $\Delta^* = 500$.

5 The anomalies

Barros Oliveira et al [15] show that the CSW potential has anomalies in density, diffusion and structure following the hierarchy reported for other two-scale potentialsand for the SPC/E water. With our systematic study of the parameter controlling the CSW potential, we show the relation between the slope of the shouldered-well and the different anomalous regions.

5.1 The density anomaly

For all tested values of Δ^* we find a temperature of minimum pressure along the isochores near the L-L critical points (Fig. 3). This temperature correspond to a temperature of maximum density (TMD) at constant P. We find that the region where density has this anomalous behaviour (ρ decreasing for decreasing T) shrinks for increasing Δ^* and tends to collapse in one single point in the $P^* - T^*$ plane for $\Delta^* \to \infty$, aproximating the discontinuous case (Fig. 7).

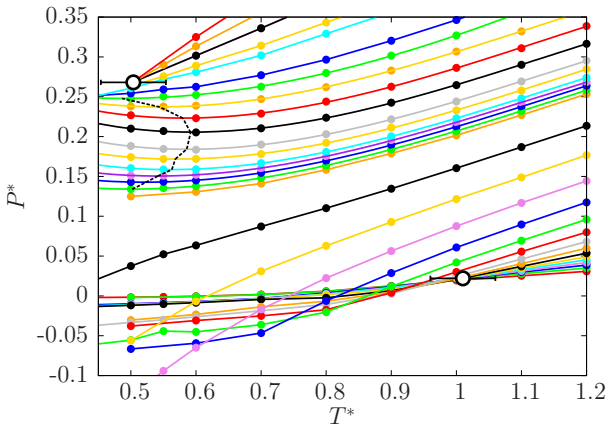

Figure 3: The $P^* - T^*$ phase diagram for $\Delta^* = 30$. Isochores correspond, from bottom to top at $T^* = 1.2$, to densities $\rho^* = 0.04$, 0.05, 0.06, 0.07, 0.08, 0.09, 0.10, 0.11, 0.12, 0.13, 0.14, 0.15, 0.16, 0.17, 0.18, 0.19, 0.19125, 0.1925, 0.19375, 0.195, 0.1975, 0.20, 0.205, 0.21, 0.215, 0.22, 0.225, 0.23, 0.235, 0.24, 0.25, 0.26 and 0.27. The points where isochores cross correspond to the G-L and L-L critical points (empty circles). The black dotted line is a guide for the eye estimating the TMD line, correspondig to the line of minima along the isochores.

5.2 Diffusion anomaly

Normal fluids show monotonic decrease in the diffusion coefficient as density is increased at constant T. For the family of potentials given by Eq (1) we find an anomalous-diffusion region, i.e. a region $\rho_{Dmin} < \rho < \rho_{Dmax}$ where D increases with density at constant T (Fig. 4). The diffusion coeficient is calculated from the mean square displacement

$$\langle \Delta r(t)^2 \rangle = \langle [r(t_o + t) - r(t_o)]^2 \rangle \qquad (2)$$

taking the long time limit

$$D = \lim_{t\to\infty} \frac{< \Delta r(t)^2 >}{2dt} \qquad (3)$$

where $d = 3$ is the dimension of the system. We find that similarly to the density anomaly, the region of diffusion anomally shrinks as Δ^* increases, always including the TMD line between ρ_{Dmin} and ρ_{Dmax} as it tends to a single point (Fig. 7).

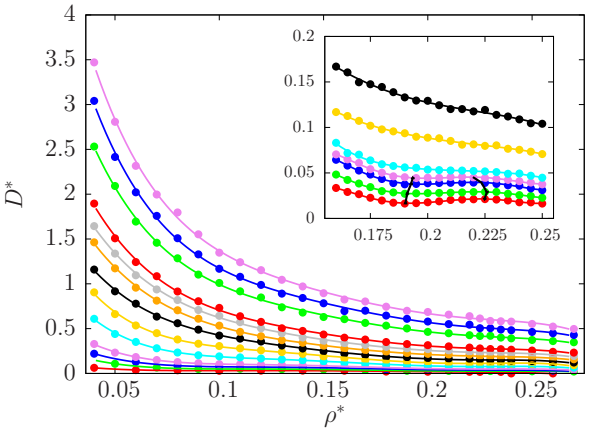

Figure 4: Diffusion coefficient in terms of density for diferent isotherms, corresponding to temperatures, from top to bottom, of $T^* = 0.45$, 0.5, 0.55, 0.6, 0.7, 0.8, 0.9, 1.0, 1.1, 1.2, 1.5, 1.7 and 1.9, for $\Delta^* = 30$. Inset: region where diffusion anomaly occurs with T^*, from top to bottom, 0.45, 0.5, 0.55, 0.57, 0.6, 0.7 and 0.8. Black solid line delimites the region where D grows for increasing density between $\rho^*_{Dmin} < \rho^* < \rho^*_{Dmax}$, that is, the region where particles move faster under compression.

5.3 Structural anomaly

The structural behaviour of the system is studied in terms of the translational order parameter t and the orientational order parameter Q_6. The translational order parameter is defined as [10],[13], [39]

$$t \equiv \int_0^{\xi_c} |g(\xi) - 1| d\xi \tag{4}$$

where ξ is a reduced distance (in units of the mean interparticle separation $\rho^{-1/3}$) given by $\xi \equiv r\rho^{1/3}$,ξ_c is the reduced cuttoff distance and $g(\xi)$ is the radial distribution function. As the parameter t depends only on the deviations of $g(\xi)$ from unity its value is sensible to long range periodicities. For an ideal gas $g(\xi)$ is constant and equal to 1 and there is no translational order ($t = 0$). For a cristal phase $g(\xi) \neq 1$ for long distances and t becomes large. While normal fluids show a monotonic increase in t with density, the potential Eq. (1) presents a density of maximum t from which the translational order decreases until it reaches a density of minimum t, where it recovers the normal behaviour (Fig. 5).

Local orientational order for a particle i is defined as [14]

$$Q_l^i = \left[\frac{4\pi}{2l+1} \sum_{m=-l}^{m=l} |(\bar{Y}_{lm}^i)_k|^2 \right]^{1/2} \tag{5}$$

where Y_{lm} are the spherical harmonics evaluated over the projections on the unit sphere of the vectors $r_{ij}(\theta_{ij}, \phi_{ij})$ in

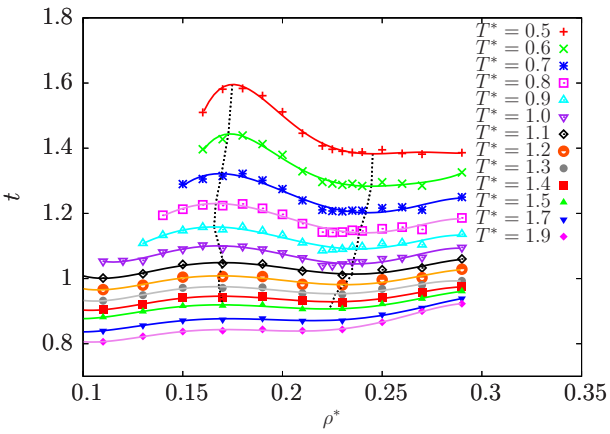

Figure 5: Translational order parameter vs. density shown for $\Delta^* = 30$. Black dotted lines joining the maxima and minima in the isotherms are a guide for the eye delimiting the region where t decreases anomalously.

spherical coordinates (r,θ,ϕ) that connect particle i with its k nearest neighbours j, for which the average $(\bar{Y}_{lm}^i)_k \equiv \frac{1}{k}\sum_{j=1}^{k} Y_{lm}(r_{ij})$ is taken. Global order is obtained by averaging local order over all particles

$$Q_l = \frac{1}{N} \sum_{i=1}^{N} Q_l^i \tag{6}$$

We study the case $l = 6$ and $k = 12$ nearest neighbours [40]. Q_6 is a good quantity for evaluating deviations of the angular positions of the 12 neighbours with respect to the f.c.c arrangement, with $Q_6^{fcc} = 0.574$ for f.c.c, and $Q_6^{ih} = 1/\sqrt{k} = 0.287$ (k=12) for an isotropic homogeneous system.

The calculations involved in the evaluation of Q_6 can be computationally expensive. In order to reduce the computational effort we express the spherical harmonics in terms of the Legendre Polynomials P_l obtaining

$$Q_l^s = \frac{1}{\sqrt{k}} \left[1 + \frac{2}{k} \sum_{i=1}^{k-1} \sum_{j=i+1}^{k} P_l(\cos\gamma_{ij}^s) \right]^{1/2} \tag{7}$$

For $l = 6$ and $k = 12$ we have

$$Q_6^s = \frac{1}{\sqrt{12}} \left[1 + \frac{1}{6} \sum_{i=1}^{11} \sum_{j=i+1}^{12} P_6(\cos\gamma_{ij}^s) \right]^{1/2} \tag{8}$$

where the sixth order Legendre Polynomial is given by $P_6(x) = \frac{1}{16}\left(231x^6 - 315x^4 + 105x^2 - 5\right)$.

The normal beahviour of Q_6 for a fluid without anomalies is to increase monotonically when density increases at constant T. Q_6 gets higher values as the system is cooled, showing the tendency of the molecules to arrange in ordered orientations as we reach the crystal phase. If temperature is increased, Q_6 decreases to its value Q_6^{ih}. The potential studied here has a nonmonotonic behaviour along the isotherms increasing ρ showing a maximum at ρ_{Qmax} (Fig. 6).

The density ρ_{Qmax} for each isotherm lies between ρ_{tmax} and ρ_{tmin}, the region where t also behaves anomalously.

	T^*_{L-G}	P^*_{L-G}	ρ^*_{L-G}	T^*_{L-L}	P^*_{L-L}	ρ^*_{L-L}
$\Delta^* = 15$	0.95 ± 0.06	0.019 ± 0.008	0.08 ± 0.03	0.49 ± 0.01	0.285 ± 0.007	0.247 ± 0.008
$\Delta^* = 30$	1.01 ± 0.07	0.022 ± 0.008	0.08 ± 0.03	0.50 ± 0.01	0.267 ± 0.005	0.255 ± 0.009
$\Delta^* = 100$	1.06 ± 0.04	0.025 ± 0.005	0.08 ± 0.03	0.53 ± 0.02	0.243 ± 0.005	0.262 ± 0.008
$\Delta^* = 300$	1.06 ± 0.05	0.027 ± 0.009	0.09 ± 0.02	0.51 ± 0.01	0.231 ± 0.007	0.271 ± 0.008
$\Delta^* = 500$	1.08 ± 0.06	0.027 ± 0.008	0.09 ± 0.03	0.52 ± 0.01	0.204 ± 0.007	0.272 ± 0.008
DSW	1.24 ± 0.01	0.030 ± 0.001	0.09 ± 0.02	0.69 ± 0.02	0.110 ± 0.002	0.280 ± 0.020

Table 1: Temperatures T^*_{L-G} and T^*_{L-L}, pressures P^*_{L-G} and P^*_{L-L}, densities ρ^*_{L-G} and ρ^*_{L-L} (in reduced units) corresponding to the critical points C_{L-G} and C_{L-L} respectivelly, for the different values of Δ^* studied in this work. The coordinates of the critical points for the DSW potential have also been included, corresponding to the parameters $U_R/U_A = 2$, $w_R/a = 0.6$ and $w_A/a = 0.7$. The data for $\Delta^* = 15$ has been obtained from Ref. [1],[15]

In the area between ρ_{Qmax} and ρ_{tmin} both order parameters decrease for increasing ρ, hence the liquid gets more diordered with increasing density. This behaviour defines the structural anomalous region $\rho_{Qmax} \leq \rho \leq \rho_{tmin}$.

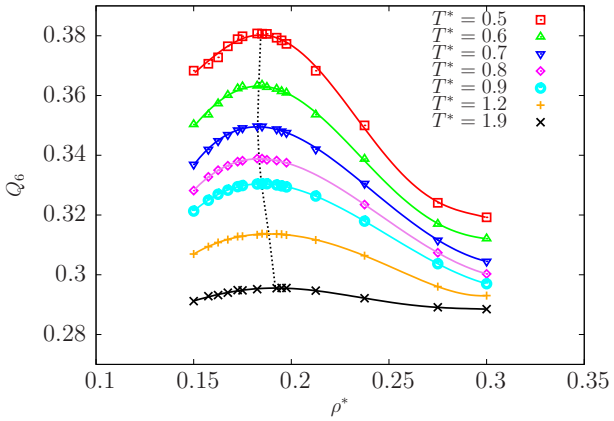

Figure 6: Orientational order parameter Q_6 vs density for $\Delta^* = 30$. Dotted line is a guide for the eye joining the maxima along the isotherms. Errorbars are smaller than symbols' size.

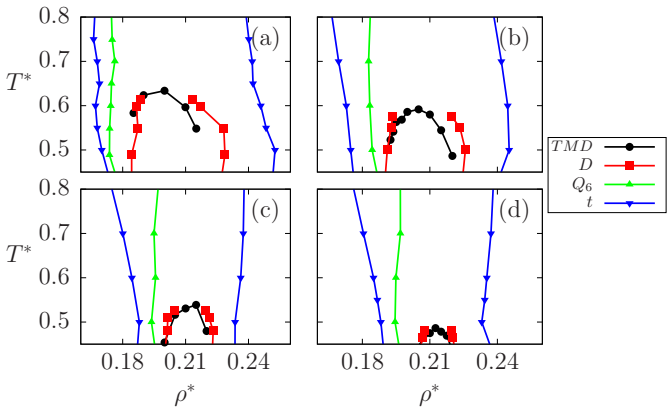

Figure 7: Hierarchy of anomalies in the $T^* - \rho^*$ plane, plotted for $\Delta^* = 15$ (a), $\Delta^* = 30$ (b), $\Delta^* = 100$ (c) and $\Delta^* = 500$ (d). As the value of Δ^* increases, both the regions of density and diffusion anomalies contract to narrower ranges of temperature and density, the later allways encompassing the TMD line. Structural anomalous region also contracts, but tends assimptotically to finite values.

By increasing the value of Δ^* we find that the structural anomalous region contracts in the $T^* - \rho^*$ plane (Fig. 7). At variance with the other anomalies, the structural anomaly does not shrink toward a single point, but tends assimptotically to a fixed region. Although a detailed study of the structural anomalous region of the DSW potential has not been performed yet, *Barros de Oliveira et al* [15] predicted, by arguments of estimators derived from the excess entropy, that the discontinuos potential should present the structural anomaly. This prediction is consistent with our results showing that the boundaries of the structural-anomalous region tend to a limiting value for ρ_{Qmax} and ρ_{tmin}.

5.4 Estimations through the excess entropy

The excess entropy s^{ex} is defined as the difference between the entropy s of a real fluid at a given T and ρ and the entropy of an ideal gas s^{ig} under the same conditions $s^{ex} = s - s^{ig}$, and quantifies the entropy due to interactions and correlations between the particles of the fluid. There exists a relation between the behaviour of the excess entropy and the aparition of anomalies in density, diffusion and structure. Errington *et al* [44] proposed a way of estimating the different regions of anomalies studing the nonmonotonic behaviour of the excess entropy through its derivative in terms of the logarithm of density $\Sigma_{ex} \equiv (\partial s^{ex}/\partial \ln \rho)_T$. According to its criteria, the condition under which the density anomaly appears is given by $\Sigma_{ex} > 1$. The diffusion anomaly can also be predicted, following Rosenfeld's empirical parametrization [42], by the value of the estimator $\Sigma_{ex} > 0.42$. Structural anomaly is determined for $\Sigma_{ex} > 0$ (that is, the region between maxima and minima of s^{ex} as function of density), as for normal fluids the excess entropy is allways decreasing when density is increased isothermically.

The evaluation of the excess entropy migth be computationallly expensive. However, it can be aproximated directly by the two-body contribution term s_2, which depends only on the radial distribution function as

$$s_2 = -2\pi\rho \int [g(r) \ln g(r) - g(r) + 1] r^2 dr \qquad (9)$$

and represents the dominant contribution to the excess entropy [42]– [45] (between 85% and 95% of s^{ex} for a Lennard-Jones fluid [45], [46]). However $s^{ex} < s_2$ hence $\Sigma_{ex} < \Sigma_2$ where $\Sigma_2 \equiv (\partial s_2/\partial \ln \rho)_T$. Therefore, the criteria

$\Sigma_2 < 0$, $\Sigma_2 < 0.42$ and $\Sigma_2 < 1$ overestimate the regions of density, diffussion and structural anomalies, respectivelly (with about 30% uncertainty, according to Rosenfeld [41]). These criteria can be understood as a first exploration of the anomalous regions of the potential in order to predict whether a given anomally will appear in the model under examination. From this starting point, a deeper study shall be performed calculating the behaviour of the different parameters as described above.

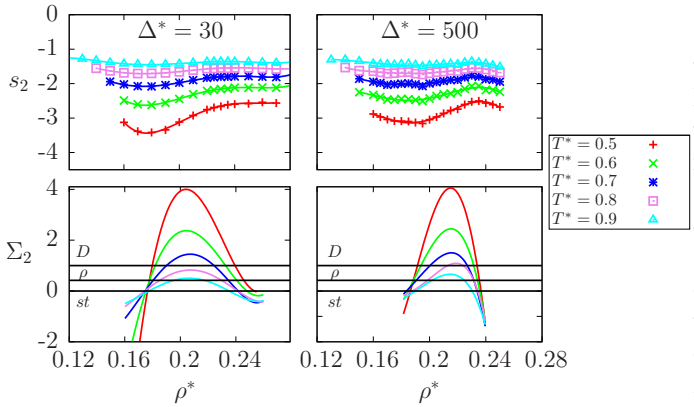

Figure 8: Excess entropy s_2 and its derivative with respect to the logarithm of density Σ_2 for the potentials corresponding to $\Delta^* = 30$ (left panels) and $\Delta^* = 500$ (right panels). Horizontal solid lines in the bottom panels are the tresholds for Σ_2 making the criteria for the anomalies (from top to bottom for diffusion, density and structure). It is important to remember that this criteria overestimate the regions of anomalies.

The predictions obtained by the evaluation of Σ_2 for the different values of Δ^* is in accordance with the results obtained directly from the simulations (Fig. 8). We observe that the predicted regions of anomalies get narrow as the slope Δ^* increases, consistent with the results obtained from our detailed simulations.

6 Discussion and conclusions

We study here the CSW potential in Eq.(1) by varying sistematically the slope of the repulsive shoulder, from soft ($\Delta^* = 15$) to sharp ($\Delta^* = 500$), aproaching the discontinuous case (DSW).

The phase diagrams ($P^* - \rho^*$ and $P^* - T^*$) for every studied case display the same general behaviour. Two first order phase transitions appear, corresponding to the L-G phase transition at low densities and a L-L phase transition at higher densities, both ending in a critical point (Table. 1).For increasing Δ^* the critical points aproximate the values for the discontinuous potential (DSW) that can be considered as a limiting case of the CSW.

The $P^* - \rho^*$ projections of the phase diagrams have a region where low temperature isotherms cross, making the anomaly in density. Accordingly, a range of isochores in the $P^* - T^*$ planes show a non-monothonic behaviour and have minimae along the TMD line. For increasing Δ^* the region of density anomaly narrows and tends to disapear. However, the L-L critical point remains present once the TMD line collapses, which shows that the presence of a L-L critical point does not necessary need the anomaly in density [1].

We find that also the region of difusion anomaly contracts for high values of Δ^*. The difusion anomalous region always includes the TMD as it shrinks.

Finally, we see that the region of structural anomaly is always present, slightly contracting toward a limiting finite region without disapearing and always including the other regions of anomalies. The hierarchy of anomalies is then always the same as for water.

We find that the excess entropy analysis is in agreement with the results from our simulations. However, the behaviour of Σ_2 for the DSW potential is still far from what we obtain for $\Delta^* = 500$, the highest studied value of the repulsive slope.

As a final remark we observe the importance of the different distances of the potential. The range of densities where anomalies appear is, aproximatelly, $0.17 < \rho^* < 0.25$, which correspond to an average distance of $1.6 < r/a < 1.8$. For this distances the discontinuous case is constant while the continuous cases have a soft repulsion. When the slope Δ is small, fluctuations over the mean energy per particle let them penetrate the shouldered region and the system has a high number of accessible states. For stronger slopes, the energy barrier to overcome for reaching shorter distances becomes greater and less states are accesible by fluctuations, making the anomalies less accessible. In conclusion, anomalies depend on the slope of the shoulder, i.e. on its sofftness. In particular, the density anomaly disappears in the limiting case of a discontinuous potential. The L-L critical point however, is a consequence of the competition between two characteristic distances and does not depend on the softness of the potential [47].

References

[1] G. Franzese, J.Mol.Liq **136**, 267 (2007).

[2] C. A. Angell, E. D. Finch, and P. Bach, J. Chem. Phys. **65**, 3065 (1976).

[3] Periodic Table of elements (http://periodic.lanl.gov/default.htm, 2007).

[4] H. Thurnd J. Ruska, J Non-Cryst. Solids **22**, 331 (1976).

[5] G. E. Sauer and L. B. Borst, Science **158**, 1567 (1976).

[6] S. J. Kennedt and J. C. Wheeler, J. Chem. Phys. **78**, 1523 (1983).

[7] T. Tsuchiya,, J. Phys. Soc. Jpn. **60**, 227 (1991).

[8] C. A. Angell, R. F. Bressel, M. Hermmatti, E. J. Sare, and J. C. Tucker, Phys. Chem. Chem. Phys. **2**, 1559 (2000).

[9] R. Sharma, S. N. Chakraborty, and C. Chakravarty, J. Chem. Phys. **125**, 204501 (2006).

[10] M. S. Shell, P. G. Debenedetti, and A. Z. Panagiotopoulos, Phys. Rev. E **66**, 011202 (2002).

[11] P. H. Poole, M. Hemmati, and C. A. Angell, Phys. Rev. Lett. **79**, 2281 (1997).

[12] S. Sastry and C. A. Angell, Nat. Mater. **2**, 739 (2003).

[13] J. R. Errington and P. D. Debenedetti, Nature (London) **409**, 318 (2001).

[14] P. J. Steinhardt, D. R. Nelson, and M. Ronchetti, Phys Rev. B **28**, t85 (1983).

[15] A. B. de Oliveira, G. Franzese, P. A. Netz, M. C. Barbosa, (2008).

[16] G. Franzese, H.E. Stanley, J. Phys., Condens. Matter **19**, 205126 (2002).

[17] G. Franzese, H.E. Stanley, Physica, A **314** 508 (2002).

[18] G. Franzese, M.I. Marques, H.E. Stanley, Phys. Rev., E Stat. Phys. Plasmas Fluids Relat. Interdiscip. Topics **67** 011103 (2003).

[19] P. Debenedetti, J. Phys., Condens. Matter **15** R1669 (2003).

[20] P.C. Hemmer, G. Stell, Phys. Rev. Lett. **24** 1284 (1970);
G. Stell, P.C. Hemmer, J. Chem. hys. **56** 4274 (1972).

[21] P.G. Debenedetti, Metastable liquids: concepts and principles (Princeton University Press, Princeton, 1998); Hydration processes in biology. Theoretical and Experimental Approaches, vol. 305 of NATO Advanced Studies Institute Series A: Life Sciences, edited by M.C. Bellisent-Funl (IOS Press, Amsterdam, 1998).

[22] M. Silbert, W.H. Young, Phys. Lett. **58A** 469 (1976);
D. Levesque, J.J. Weis, Ibid **60A** 473 (1977);
J.M. Kincaid, G. Stell, Ibid **65A** 131 (1978).

[23] W.M. Shyu, J.H. Wehling, M.R. Cordes, G.D. Gaspari, Phys. Rev., B **4** 1802 (1971).

[24] J.M. Lawrence, M.C. Croft, R.D. Parks, Phys. Rev. Lett. **35** 289 (1975)

[25] P.G. Debenedetti, V.S. Raghavan, S.S. Borick, J. Phys. Chem. **95** 4540 (1991).

[26] F.H. Stillinger, T. Head-Gordon, Phys. Rev., E Stat. Phys. Plasmas Fluids Relat. Interdiscip. Topics **47** 2484 (1993).

[27] S.S. Borick, P.G. Debenedetti, S. Sastry, J. Phys. Chem. **99** 3781 (1995);
T.M. Truskett, P.G. Debenedetti, S. Sastry, S. Torquato, J. Chem. Phys. **111** 2647 (1999).

[28] M.R. Sadr-Lahijany, A. Scala, S.V. Buldyrev, H.E. Stanley, Phys. Rev. Lett. **81** 4895 (1998), Phys. Rev., E Stat. Phys. Plasmas Fluids Relat. Interdiscip. Topics **60** 6714 (1998);
A. Scala, M.R. Sadr-Linhijany, N. Giovambattista, S.V. Buldyrev, H.E. Stanley, Ibid **63** 041202 (2001);
J. Stat. Phys. **100** 97 (2000).

[29] E.A. Jagla, Phys. Rev., E Stat. Phys. Plasmas Fluids Relat. Interdiscip. Topics **58** 1478 (1998);
J. Chem. Phys. **110** 451 (1998);
J. Chem. Phys. **111** 8980 (1998); Phys. Rev., E Stat. Phys. Plasmas Fluids Relat. Interdiscip. Topics **63** 061501 (1998);
Phys. Rev., E Stat. Phys. Plasmas Fluids Relat. Interdiscip. Topics **63** 061509 (1998).

[30] N.B. Wilding, J.E. Magee, Phys. Rev., E Stat. Phys. Plasmas Fluids Relat. Interdiscip. Topics **66** 031509 (2002); H.M. Gibson, N.B. Wilding, Phys. Rev., E Stat. Phys. Plasmas Fluids Relat. Interdiscip. Topics **74** 019903 (2006).

[31] J.B. Caballero, A.M. Puertas Phys. Rev., E Stat. Phys. Plasmas Fluids Relat. Interdiscip. Topics **74** 051506 (2006).

[32] F.H. Stillinger, T.A. Weber, J. Chem. Phys. **68** 3837 (1978).

[33] G. Franzese, G. Malescio, A. Skibinsky, S.V. Bulderev, H.E. Stanley, Nature **409** 692 (2001).

[34] G. Franzese, G. Malescio, A. Skibinsky, S.V. Bulderev, H.E. Stanley, Phys. Rev., E Stat. Phys. Plasmas Fluids Relat. Interdiscip. Topics **66** 051206 (2002).

[35] A. Skibinsky, S.V. Bulderev,G. Franzese, G. Malescio, H.E. Stanley, Phys. Rev., E Stat. Phys. Plasmas Fluids Relat. Interdiscip. Topics **69** 061206 (2004).

[36] G. Franzese, G. Malescio, A. Skibinsky, S.V. Bulderev, H.E. Stanley, Phys. Rev., E Stat. Phys. Plasmas Fluids Relat. Interdiscip. Topics **71** 061504 (2005).

[37] D. Frenkel and B. S,it, Understanding Molecular Simulation, 1st ed. (Academic, San Diego, 1996).

[38] M.P. Allen, D.J. Tidesley, Computer Simulation of Liquids, Oxford University Press, New York, 1989.

[39] J.E. Errington, P.G. Debenedetti, and S. Torquato, J. Chem. Phys. **118**, 2256 (2003).

[40] A. B. de Oliveira, P.A. Netz, T. Colla, and M.C. Barbosa, J. Chem. Phys. **125**, 124503 (2006).

[41] J.R. Errington, T.M. Truskett, and J. Mittal, J. Chem. Phys. **125**, 244502 (2006).

[42] Y. Rosenfeld, J. Phys.: Condens. Matter **11**, 5415 (1999).

[43] H.S. Green, The Molecular Theory of Fluids (North-Holland, Amsterdam, 1952).

[44] H. J. Raveché, J. Chem. Phys. **55**, 2242 (1971).

[45] A. Baranyai and D.J. Evans, Phys Rev. A **40**, 3817 (1989).

[46] S. N. Chakraborty and C. Chakravarty, J chem. Phys. **124**, 014507 (2006).

[47] J. N. Glosli, F.H. Ree, Phys. Rev. Lett. **82** 4649 (1999).